

# ON THE INVERSE KINEMATICS OF A FRAGMENT OF PROTEIN BACKBONE

Guanfeng Liu<sup>†</sup>, R.J. Milgram<sup>‡</sup>, A. Dhanik<sup>†</sup>, J.C. Latombe<sup>†</sup>

<sup>†</sup> *Department of Computer Science, Stanford University*

<sup>‡</sup> *Department of Mathematics, Stanford University*

{liugf,ankur,latombe}@cs.stanford.edu and milgram@math.stanford.edu

**Abstract** This paper studies the structure of the inverse kinematics (IK) map of a fragment of protein backbone with 6 torsional degrees of freedom. The images (critical sets) of the singularities of the orientation and position maps are computed for a slightly idealized kinematic model. They yield a decomposition of  $SO(3)$  and  $\mathcal{R}^3$  into open regions where the number of IK solutions is constant. A proof of the existence of at least one 16-solution cell in  $\mathcal{R}^3 \times SO(3)$  is given and one such case is shown.

**Keywords:** Protein backbone, inverse kinematics, critical sets.

## 1. Introduction

A protein (Creighton, 1993) is a sequence of amino-acids connected by peptide bonds. It is often modeled as a serial linkage, the *backbone*, with short side-chains. Each amino-acid contributes three atoms – N,  $C_\alpha$ , and C – and two torsional degrees of freedom (dofs) to the backbone (Fig. 1). These dofs correspond to the dihedral angles  $\phi$  and  $\psi$  around the N– $C_\alpha$  and the  $C_\alpha$ –C bonds. The inverse kinematics of the backbone is of considerable interest in biology (Coutsias et al, 2004).

Let  $F$  be a backbone fragment with 6 dihedral angles  $\phi$  and  $\psi$ , and  $f$  be its forward kinematics. It is well-known that the number of solutions of the inverse kinematics (IK) map  $f^{-1}$  has 16 as an upper bound, but it has often been questioned whether this bound is tight (Coutsias et al, 2004). Available algorithms only compute these solutions for *given* poses of the moving frame  $T$  of  $F$ . Here, we study the *global* structure of  $f^{-1}$  over the entire 6-D manifold of poses of  $T$  in  $\mathcal{R}^3 \times SO(3)$ . The images of the singularities of  $f$  are the *critical* poses, which, according to the Morse-Sard theorem, decompose the noncritical part of the image into open regions, such that in each region  $E$ ,  $f^{-1}(x)$  for each  $x \in E$  contains the same number of points. These decompositions of the 6-D manifold can be very complex, so we study the position map  $p$  and an orientation map  $\rho$  separately. It turns out  $\rho$  is quite easy to understand and the original question reduces to studying the projection to  $\mathcal{R}^3$  from

the inverse images of  $\rho$ . Given the frame associated to  $T$ , the set of configurations that give the frame is either a copy of  $(S^1)^3$  or a copy of the disjoint union  $(S^1)^3 \sqcup (S^1)^3$ . Focusing on these  $(S^1)^3$ , we can compute  $p^{-1}$  more efficiently and we find regions with 16 inverse image points. This result is reasonable since a 6-dof protein fragment does not satisfy any of the conditions under which the IK of a 6-dof serial linkage has less than 16 solutions (Mavroidis and Roth, 1994).

## 2. Kinematic Model of a Protein Fragment

Let  $F$  be a 6-dof fragment of a protein backbone as illustrated in Fig. 1. The coordinates of  $F$  are the 3 dihedral angles  $\phi_i$  around the bonds  $N^i - C_\alpha^i$ , and the 3 dihedral angles  $\psi_i$  around the bonds  $C_\alpha^i - C^i$ . For convenience, we rename  $\phi_i$  by  $\theta_{2i-2}$  and  $\psi_i$  by  $\theta_{2i-1}$ , so each conformation of  $F$  is specified by a 6-tuple  $\theta = (\theta_1, \dots, \theta_6) \in (S^1)^6$ .

We represent  $F$  by a kinematically equivalent sequence of 3 identical units, each made of two perpendicular links, a “long” one of length  $\ell_2$  and a “short” one of length  $\ell_1$ , as shown in Fig. 2. We number the links  $1, 2, \dots, 6$ , so that each link  $2i - 1$  is a long link and each link  $2i$  is a short link. Angle  $\theta_{2i-1}$  rotates short link  $2i$  about long link  $2i - 1$ . So, each short link moves in a plane perpendicular to the preceding long link. Angle  $\theta_{2i}$  rotates the long link  $2i + 1$  about an axis parallel to long link  $2i - 1$  and passing through the extremity of short link  $2i$ . Link  $2i + 1$  makes the constant angle  $\alpha = 19$  degrees with the plane perpendicular to link  $2i - 1$ . Finally, we add a long link 7 to  $F$ . This is the link associated with the moving frame  $T$ .

We summarize these remarks and put them into a mathematical setting as follows. Set

$$R_i = \begin{bmatrix} \cos(\theta_i) & -\sin(\theta_i) & 0 \\ \sin(\theta_i) & \cos(\theta_i) & 0 \\ 0 & 0 & 1 \end{bmatrix}, \quad L = \begin{bmatrix} -\sin(\alpha) & 0 & \cos(\alpha) \\ 0 & -1 & 0 \\ \cos(\alpha) & 0 & \sin(\alpha) \end{bmatrix},$$

where  $\alpha \sim .105556\pi$  is fixed and  $L^T = L^{-1} = L$ . Then, the orientations of the frames are given by

$$O_1 = I_{3 \times 3}, \quad O_{2i} = O_{2i-1}R_{2i-1}, \quad O_{2i+1} = O_{2i}R_{2i}L,$$

and  $f$  is the composition of  $p$  and  $\rho$  with

$$p: (S^1)^6 \rightarrow \mathcal{R}^3, \quad \theta \rightarrow (R_{1;2}L + R_{1;2}LR_{3;4}L)v_1 + (R_1 + R_{1;2}LR_3 + R_{1;2}LR_{3;4}LR_5)v_2, \quad (1)$$

$$\rho: (S^1)^6 \rightarrow SO(3), \quad \theta \rightarrow R_{1;2}LR_{3;4}LR_{5;6}L, \quad (2)$$

where  $R_{i;j} = R_i R_j$ ,  $v_1 = [0, 0, \ell_2]^T$ , and  $v_2 = [\ell_1, 0, 0]^T$ .

This paper studies the structure of the inverse kinematics  $f^{-1} = (p, \rho)^{-1}$ . Noticing that for any  $(X, R) \in \mathcal{R}^3 \times SO(3)$ ,

$$(p, \rho)^{-1}(X, R) = p^{-1}(X) \cap \rho^{-1}(R),$$

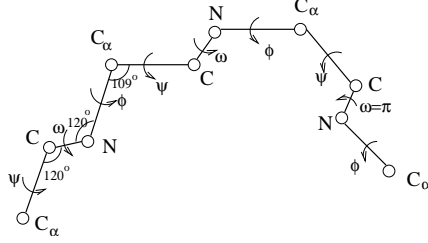


Figure 1. 6-dof fragment

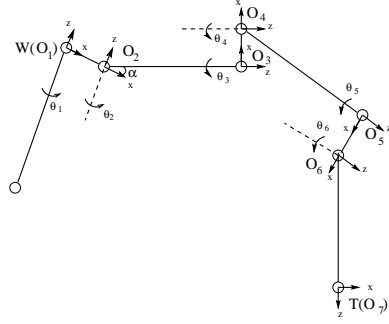


Figure 2. Equivalent model

we proceed in two steps. First, we derive the inverse orientation map  $\rho^{-1} : SO(3) \rightarrow (S^1)^6$  and show that in general  $\rho^{-1}(R)$  is the disjoint union of two 3-D tori  $\mathcal{M}_1$  and  $\mathcal{M}_2$ . Next, we compute  $p_k^{-1}(X)$ , where  $p_k$ ,  $k \in 1, 2$ , is the map  $p$  with its domain restricted to  $\mathcal{M}_k$ .

### 3. Inverse Orientation Map

**Reduction.** In Eq. (2) only the sums  $\theta_{2i-1} + \theta_{2i}$  appear. So, we write  $\tau_i = \theta_{2i-1} + \theta_{2i}$ ,  $i = 1, 2, 3$ , and  $\tau = (\tau_1, \tau_2, \tau_3)$ . As  $\theta$  runs over  $(S^1)^6$ ,  $\tau$  runs over the 3-D torus  $(S^1)^3$ , and  $\rho$  factors as composition

$$\rho = \hat{\rho} \circ (+) : (S^1)^6 \rightarrow (S^1)^3 \rightarrow SO(3)$$

where  $\hat{\rho} : (S^1)^3 \rightarrow SO(3)$ ,  $\tau \rightarrow R_{\tau_1} L R_{\tau_2} L R_{\tau_3} L$ .  $R_{\tau_i}$  is the rotation of angle  $\tau_i$  around the  $z$  axis. Given  $R \in SO(3)$ , the values of  $\hat{\rho}^{-1}(R)$  are the solutions of  $\hat{\rho}(\tau) := R_{\tau_1} L R_{\tau_2} L R_{\tau_3} L = R$ , which is equivalent to:

$$\hat{\rho}(\tau)L := R_{\tau_1} L R_{\tau_2} L R_{\tau_3} L = RL. \quad (3)$$

Since  $\hat{\rho}(\tau)L$  defines the frame on the  $z$ -axis, (which is fixed by  $R_{\tau_3}$ , we further reduce Eq. (3) by eliminating the variable  $\tau_3$ . To do this, we define  $A_z : SO(3) \rightarrow S^2$ ,  $R \rightarrow Rz$ , where  $z = [0, 0, 1]^T$  and  $S^2$  denotes the unit 2-D sphere. Since  $A_z(R_{\tau_3}) = z$ , applying  $A_z$  to both sides of Eq. (3) yields:

$$A_z(\hat{\rho}(\tau)L) := R_{\tau_1} L R_{\tau_2} L z = RLz \quad (4)$$

where  $R_{\tau_1} L R_{\tau_2} L$  defines the orientation of the  $z$ -axis of frame 6 in  $W$ . We can solve this equation for  $(\tau_1, \tau_2)$ . The value of  $\tau_3$  is then uniquely determined by:

$$R_{\tau_3} = (R_{\tau_1} L R_{\tau_2} L)^T RL. \quad (5)$$

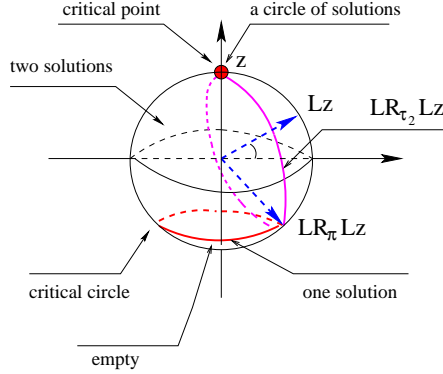


Figure 3. Critical set of  $\eta$

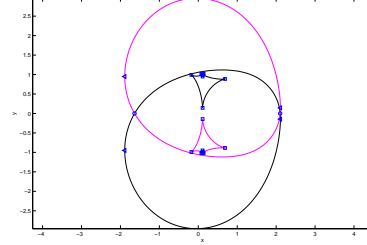


Figure 4. The discriminant curve  $\mathcal{X}_d$  computed with  $\gamma = \pi$  and  $d = -0.32$ .

To each solution  $\tau = (\tau_1, \tau_2, \tau_3)$  of Eqs. (4) and (5) corresponds a set of values of  $\theta = (\theta_1, \dots, \theta_6)$  such that  $\theta_{2i-1} + \theta_{2i} = \tau_i$  for  $i = 1, 2, 3$ . This set is a 3-D torus  $(S^1)^3$ .

**Singular set.** The singularities of  $\hat{\rho}$  are the points in  $(S^1)^3$  where the  $3 \times 3$  Jacobian matrix  $J\hat{\rho}$  has rank less than 3. When working with Lie groups, the Jacobian is  $(d\hat{\rho})\hat{\rho}^{-1}$ . This gives a map to the Lie algebra. The Lie algebra of  $SO(3)$  is 3-dimensional and a change of basis gives  $J\hat{\rho} = [z, R_{\tau_1}Lz, R_{\tau_1}LR_{\tau_2}Lz]$ ,  $z$  as above.  $J\hat{\rho}$  has at least rank 2. It has rank exactly 2 if and only if:  $\det(J\hat{\rho}) = \sin(\tau_2) \cos(\alpha) = 0$ . As  $\cos(\alpha) \neq 0$ , the singular set of  $\hat{\rho}$  is  $\{\tau \mid \tau_2 = 0\} \cup \{\tau \mid \tau_2 = \pi\}$ .

**Critical set and number of solutions.** The quotient map  $\eta : (S^1)^3 \rightarrow SO(3) \rightarrow S^2$  that appears in the left-hand side of Eq. (4), has the same singular set as  $\hat{\rho}$ . The critical set of  $\eta$  – i.e., the image of  $\{\tau \mid \tau_2 = 0\} \cup \{\tau \mid \tau_2 = \pi\}$  – is the union of  $C_1 = R_{\tau_1}R_{\tau_3}z = z$  and  $C_2 = R_{\tau_1}LR_{\pi}LR_{\tau_3}z = R_{\tau_1}LR_{\pi}Lz$  for all  $\tau_1 \in S^1$ .  $C_1$  is the point that corresponds to the situation where the  $z$ -axes of  $W$  and frame 6 are parallel. Indeed, when  $\tau_2 = 0$ , the  $z$ -axis of frame 6 is parallel to the  $z$ -axis of  $W$  for any value of  $\tau_1$ . On the other hand,  $R_{\tau_1}LR_{\pi}Lz = [(\sin(2\alpha) \cos(\tau_1), \sin(2\alpha) \sin(\tau_1), -\cos(2\alpha))]^T$ , so  $C_2$  is the circle perpendicular to the  $z$ -axis and passing through the point  $LR_{\pi}Lz$ . See Fig. 3.

The inverse map  $\eta^{-1}$ , hence  $\hat{\rho}^{-1}$ , has a constant structure in  $C_1$ ,  $C_2$ , and in each of the two open subsets of  $S^2$  bounded by  $C_1$  and  $C_2$ . We notice that:  $L(LR_{\tau_2}Lz) = [\cos(\alpha) \cos(\tau_2), \cos(\alpha) \sin(\tau_2), \sin(\alpha)]^T$ . So,  $LR_{\tau_2}Lz$  is a circle perpendicular to  $Lz$  contained in the subset of  $S^2$  be-

tween  $C_1$  and  $C_2$ , except at  $\tau_2 = 0$  and  $\tau_2 = \pi$  where it coincides with  $C_1$  and  $C_2$ , respectively (Fig. 3). For any fixed  $\tau_1 \in S^1$ , the set  $R_{\tau_1}LR_{\tau_2}Lz$  is the circle obtained by rotating  $LR_{\tau_2}Lz$  by  $\tau_1$  around the  $z$  axis. Thus, for every point  $s$  in the region between  $C_1$  and  $C_2$ ,  $R_{\tau_1}LR_{\tau_2}Lz$  contains  $s$  for two distinct values of  $\tau_1$ . We conclude that  $\eta^{-1}$  has two values  $(\tau_1^k, \tau_2^k)$ ,  $k = 1, 2$ . In  $C_1$ ,  $s = z$  and  $\eta^{-1}(s) = \{(\tau_1, 0) \mid \tau_1 \in S^1\}$ . For any  $s \in C_2$ ,  $\eta^{-1}(s)$  has a single value of the form  $(\tau_1, \pi)$ . Elsewhere  $\eta^{-1}(s)$  is empty.

Corresponding to each value  $(\tau_1, \tau_2)$  of  $\eta^{-1}(s)$  there is a unique value of  $\tau_3$  given by Eq. (5), hence a single value of  $\hat{\rho}^{-1}(R)$ . Thus, as we initialize an orientation  $R \in SO(3)$  not in the critical sets  $C_1$  and  $C_2$ ,  $\rho^{-1}(R)$  is the disjoint union of two 3-D tori, written  $\mathcal{M}_k$ ,  $k = 1, 2$ .

#### 4. Inverse Position Map

**Restriction to  $\mathcal{M}_k$ .** We now study  $p_k^{-1}(X)$ , where  $X \in \mathcal{R}^3$  and  $p_k$ ,  $k \in 1, 2$ , is the position map  $p$  with its domain restricted to  $\mathcal{M}_k$ . Since  $\theta_{2j-1} + \theta_{2j}$ ,  $j = 1, 2, 3$ , are constant on  $\mathcal{M}_k$  and equal to  $\tau_j^k$ , each point on  $\mathcal{M}_k$  is uniquely defined by the values of  $\theta_1$ ,  $\theta_3$ , and  $\theta_5$ . Eq.(1) yields:

$$p_k : (S^1)^3 \rightarrow \mathcal{R}^3, \quad (\theta_1, \theta_3, \theta_5) \rightarrow v_{0,k} + (R_1 + R_{\tau_1^k}LR_3 + R_{\tau_1^k}LR_{\tau_2^k}LR_5)v_2$$

where  $v_{0,k} = (R_{\tau_1^k}L + R_{\tau_1^k}LR_{\tau_2^k}L)v_1$  is a constant vector and  $\{R_1v_2\}$ ,  $\{R_{\tau_1^k}LR_3v_2\}$ , and  $\{R_{\tau_1^k}LR_{\tau_2^k}LR_5v_2\}$  are constant circles of radius  $\ell_1$  contained in three different planes.

Computing  $p_k^{-1}(X)$  amounts to solving the equation:

$$X' = \hat{p}_k(-\theta_2, \theta_3, \theta_5) := R_{-2}v_2 + LR_3v_2 + LR_{\tau_2^k}LR_5v_2, \quad (6)$$

where  $X' = R_{\tau_1^k}^T(X - v_{0,k})$  and  $R_{-2}$  is the rotation of  $-\theta_2$  around  $z$ .

**Critical set.** Here we directly determine the critical positions  $X'$  where the number of solutions of  $\hat{p}_k$  changes. We rewrite Eq. (6) as:

$$X' - r(w) = q(t, u), \quad (7)$$

where we rename the variables as  $t = -\theta_2$ ,  $u = \theta_3$ ,  $w = \theta_5$ , and  $\gamma = \tau_2^k$ .  $X' - r(w)$  is a unit circle centered at  $X'$  and  $q(t, u)$  spans a quartic surface  $Q$  in  $\mathcal{R}^3$ .  $Q$  is the Minkowski sum of two circles, so it is bounded and connected. Eq. 7 can be solved by computing the intersections between  $X' - r(w)$  and the cross-section curve of  $Q$  by the plane containing  $X' - r(w)$ . We compute  $r(w) = \hat{x}c_w + \hat{y}s_w$ .  $\hat{x} = [s_\alpha^2c_\gamma + c_\alpha^2, s_\gamma s_\alpha, s_\alpha c_\alpha(1 - c_\gamma)]^T$  and  $\hat{y} = [-s_\alpha s_\gamma, c_\gamma, c_\alpha s_\gamma]^T$  form an orthonormal basis for the plane

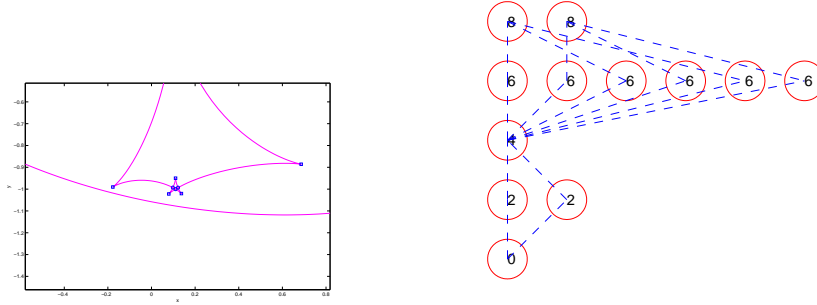


Figure 5. Zoom on a portion of  $\mathcal{X}_d$  in Fig. 4. The centers of the small squares and the small circles are cusp points and self-intersection points, respectively. Figure 6. The planar graph determined by the discriminant curve of Fig. 4. The number of solutions is shown in each node.

containing the circle  $r(w)$ . Setting  $\hat{z} = \hat{x} \times \hat{y}$ , the equation of the plane containing  $X' - r(w)$  is:

$$\hat{z}^T q = d \quad (8)$$

where  $d = \hat{z}^T X'$ . We let  $P_d$  denote the plane defined by this equation. When  $X'$  spans  $\mathcal{R}^3$ ,  $P_d$  translates, but its orientation remains constant.

On the other hand, we can easily compute:

$$q(t, u) = [c_t - s_\alpha c_u, s_t - s_u, c_\alpha c_u]^T. \quad (9)$$

By replacing  $q$  by this expression in Eq. (8), we get the equation of the cross-section  $Q_d$  of  $Q$  by  $P_d$  in terms of  $(t, u)$ :

$$c_{(u-\gamma)} + K(\gamma)s_{(t+\beta)} = \frac{d}{c_\alpha} \quad (10)$$

where  $c_\beta = -\frac{s_\gamma}{K(\gamma)}$ ,  $s_\beta = \frac{s_\alpha(1-c_\gamma)}{K(\gamma)}$ , and  $K(\gamma) = \sqrt{s_\gamma^2 + s_\alpha^2(1-c_\gamma)^2}$ .

The number of intersection points in  $Q_d \cap (X' - r(w))$  varies as  $X'$  runs over  $\mathcal{R}^3$ . The  $X'$  such that the circle is tangent to  $Q_d$  form the critical set  $\mathcal{X} \subset \mathcal{R}^3$  of  $\hat{p}_k$ . Let  $d_{\min}$  and  $d_{\max}$  be the extreme values of  $d$  between which the plane  $\hat{z}^T q = d$  and  $Q$  intersect. For any  $d \in [d_{\min}, d_{\max}]$ , the values of  $X'$  such that  $X' - r(w)$  lies in the plane  $P_d$  and is tangent to  $Q_d$  form a curve  $\mathcal{X}_d$  called the *discriminant curve* at  $d$ . The union of the discriminant curves for  $d$  in  $[d_{\min}, d_{\max}]$  is the critical surface  $\mathcal{X}$  of  $\hat{p}_k$ . Fig. 4 shows a discriminant curve, with several cusp and self-intersection points. An animation of both the cross-section of  $Q$  and the corresponding discriminant curve when  $d$  varies is available at [www.stanford.edu/~phwu1/curve](http://www.stanford.edu/~phwu1/curve) when  $\gamma = \pi$ .

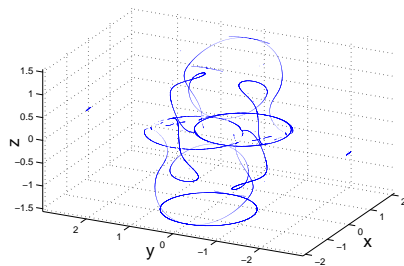


Figure 7. The cusp curves when  $\gamma = \pi$ .

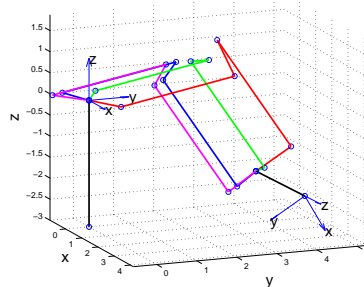


Figure 8. Four of the 16 solutions.

**Decomposition of  $\mathcal{R}^3$  into regions.** The surface  $\mathcal{X}$  decomposes  $\mathcal{R}^3$  into open 3-D regions such that the number of solutions of the inverse position map is constant over each one. We first compute the decomposition of a plane  $P_d$  by  $\mathcal{X}_d$ . Next, we partition  $[d_{min}, d_{max}]$  into smaller open intervals, such that over each such interval the discriminant curves  $\mathcal{X}_d$  are equivalent. We get the decomposition of  $\mathcal{R}^3$  by “stacking” the decompositions in the successive intervals.

*Decomposition of  $P_d$ :* We sweep a line  $L$  parallel to the  $y$ -axis across the plane  $P_d$  from left to right to construct a set  $S$  of sub-regions and their adjacency relations.  $S$  is initialized to the empty set. During the sweep, whenever  $L$  crosses a cusp point, a self-intersection point, or a vertical tangency point, sub-regions are added to  $S$  and the adjacency relation is updated. When the sweep is completed, adjacent sub-regions in  $S$  not separated by  $\mathcal{X}_d$  are merged to form the decomposition of  $P_d$ . The outcome is a planar *graph* in which the nodes are the computed regions and the edges represent the adjacency relation. The number of solutions of the inverse position map varies by 2 at each crossing of a region boundary. We compute cusp and self-intersection points numerically by approximating the discriminant curve by line segments. Fig. 6 shows the graph computed from the discriminant curve shown in Fig. 4. An animation of the discriminant curve and the corresponding graph when  $d$  varies is available at [www.stanford.edu/~phwu1/curve](http://www.stanford.edu/~phwu1/curve) when  $\gamma = \pi$ .

*Decomposition of  $\mathcal{R}^3$ :* As  $d$  varies from  $d_{min}$  to  $d_{max}$ , the planar graph in  $P_d$  changes only at a finite number of *critical* values of  $d$ , which we denote  $d_i$ ,  $i = 1, \dots, m$ . Over each open interval  $(d_i, d_{i+1})$ ,  $i = 0, \dots, m$ , with  $d_0 = d_{min}$  and  $d_{m+1} = d_{max}$ , the discriminant curves are equivalent and the planar graph remains constant. Let  $G_i$  be the planar graph in

interval  $(d_i, d_{i+1})$ . The decomposition of  $\mathcal{R}^3$  is obtained by merging every pair of regions from  $G_i$  and  $G_{i+1}$ , for all  $i = 0, \dots, m$ , that are adjacent, but not separated by  $\mathcal{X}$ . The corresponding nodes of the planar graphs are also merged to obtain the graph of the decomposition of  $\mathcal{R}^3$ .

The 2-D surface  $\mathcal{X}$  is made of smooth patches separated by cusp and self-intersection curves. The cusp (resp. self-intersection) curves are the locus  $\mathcal{X}^{\text{cusp}}$  (resp.  $\mathcal{X}^{\text{self}}$ ) of all the cusp (self-intersection) points of the discriminant curves  $\mathcal{X}_d$  when  $d$  varies. The critical values of  $d$  are contributed by  $\mathcal{X} \setminus (\mathcal{X}^{\text{cusp}} \cup \mathcal{X}^{\text{self}})$ ,  $\mathcal{X}^{\text{cusp}}$ , and  $\mathcal{X}^{\text{self}}$ . For lack of space, we do not describe their computation here. Fig. 7 shows  $\mathcal{X}^{\text{cusp}}$  for  $\gamma = \pi$ .

## 5. Existence of a 16-Solution Cell

**Theorem 1** *There exists a nonempty open region in  $\mathcal{R}^3 \times SO(3)$  such that for all  $(X, R)$  in this region,  $(p, \rho)^{-1}(X, R)$  contains 16 points.*

**Proof:** Consider first an orientation  $R_0 \in SO(3)$  that lies in the critical circle  $C_2$ .  $\rho^{-1}(R_0)$  is a copy of  $(S^1)^3$ . There is a nonempty open region  $E_0 \subset C_2$  such that for all  $R$  in  $E_0$ ,  $p(\rho^{-1}(R))$  has an open region  $U$  so that  $p^{-1}(X)$  contains 8 points for  $X \in U$  (see Fig. 6). Let  $R'$  be a noncritical orientation that is close to  $R_0$ . Then  $\rho^{-1}(R')$  is a disjoint union of two 3-D tori  $\mathcal{M}_k$ ,  $k = 1, 2$ . For each  $p_k$ , there exists a nonempty open region  $E_k$  with 8 inverse image points. Moreover, for  $R'$  sufficiently close to  $R_0$ ,  $E = E_1 \cap E_2$  is nonempty. Then  $(p, \rho)^{-1}(X, R')$  has 16 solutions for all  $X \in E$ . ■

Using the idea in the proof, we constructed the following pose  $(X, R)$  of  $T$ :

$$X = \begin{bmatrix} 1.9760 \\ 4.5809 \\ -2.2402 \end{bmatrix} \quad \text{and} \quad R = \begin{bmatrix} 0.6742 & -0.3715 & -0.6383 \\ 0.2378 & -0.7091 & 0.6638 \\ -0.6992 & -0.5993 & -0.3897 \end{bmatrix},$$

such that  $(p, \rho)^{-1}(X, R)$  contains 16 solutions (for a fragment in which  $\ell_1 = 1$  and  $\ell_2 = 3$ ). Four of them are shown in Fig. 8. (It is easily seen that the existence of 16-solution cell is independent of the link lengths as long as the short links all have the same length.)

**Acknowledgements:** This research was funded by NSF grant DMS-0443939.

## References

- Coutsias, E.A., Seok, C, Jacobson, M.P., and Dill, K.A. (2004), A kinematic view of loop closure. *J. Comp. Chem.*, 25:510–528.
- Creighton, T.E. (1993), *Proteins : Structures and molecular properties*. W. H. Freeman and Company, New York, 2nd edition.
- Mavroidis, C., and Roth, B. (1994), Structural Parameters which reduce the number of manipulator configurations. *J. Mech. Design, Trans. ASME*, vol. 116, pp. 3–10.